

Reaction Mechanisms of a Photo-Induced [1,3] Sigmatropic Rearrangement via a Nonadiabatic Pathway

Weiqliang Wu, Kunhui Liu, Chunfan Yang, Hongmei Zhao, Huan Wang, Youqing Yu, and Hongmei Su*

State Key Laboratory of Molecular Reaction Dynamics, Beijing National Laboratory for Molecular Sciences (BNLMS), Institute of Chemistry, Chinese Academy of Sciences, Beijing 100190, China

Received: July 13, 2009; Revised Manuscript Received: October 22, 2009

Time-resolved Fourier transform infrared absorption spectroscopy measurements and B3LYP/cc-pVDZ calculations have been conducted to characterize the reaction dynamics of a remarkable photoinduced 1,3-Cl sigmatropic rearrangement reaction upon 193 or 266 nm excitation of the model systems acryloyl chloride (CH_2CHCOCl) and crotonyl chloride ($\text{CH}_3\text{CHCHCOCl}$) in solution. The reaction is elucidated to follow nonadiabatic pathways via two rapid ISC processes, $S_1 \rightarrow T_1$ and $T_1 \rightarrow S_0$, and the S_1/T_1 and T_1/S_0 surface intersections are found to play significant roles leading to the nonadiabatic pathways. The $S_1 \rightarrow T_1 \rightarrow S_0$ reaction pathway involving the key participation of the T_1 state is the most favorable, corresponding to the lowest energy path. It is also suggested that the photoinduced 1,3-Cl migration reaction of RCHCHCOCl ($\text{R} = \text{H}, \text{CH}_3$) proceeds through a stepwise mechanism involving radical dissociation–recombination, which is quite different from the generally assumed one-step concerted process for pericyclic reactions.

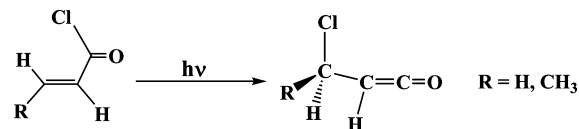
1. Introduction

As a class of important chemical reaction, pericyclic reactions have been attracting continuous research interest since the development of the general theory of orbital symmetry by Woodward and Hoffmann.¹ One of the most fascinating of these reactions is the thermal and photochemical [1, n] sigmatropic rearrangement that involves a migration of a group attached by a *sigma* bond to the terminus of an adjacent *pi* electron system.^{2–4} Not only carbon and hydrogen migrations, but also shifts of other functionalities, including halogen, nitrogen, and oxygen atoms, constitute crucial reactions in many organic and bioorganic synthesis.^{5–9}

Although numerous examples of studies on thermally induced [1, n] sigmatropic rearrangement have been documented in the literature,^{5–9} knowledge is rather limited concerning the photochemically initiated sigmatropic rearrangements due to the complications caused by the involvement of one or more excited-state surfaces and sometimes the existence of surface crossings. Taking the photoinduced 1,3-Cl sigmatropic migration of acryloyl chloride (CH_2CHCOCl) and crotonyl chloride ($\text{CH}_3\text{CHCHCOCl}$) as model systems (shown in Scheme 1), the present work aims to examine the reaction dynamics of the photochemical sigmatropic rearrangements and provide mechanistic insights into this important pericyclic reaction.

Acryloyl chloride belongs to the group of α, β unsaturated carbonyl compounds that, due to the rich photochemistry of the enone functional group, $-\text{C}=\text{C}-\text{C}=\text{O}$, serve as interesting building blocks for further functionalization in the medical and biological fields.^{10,11} Owing to the strong interactions between the neighboring $\text{C}=\text{C}$ and $\text{C}=\text{O}$ groups, CH_2CHCOCl exhibits a rich and varied photochemistry that includes α bond cleavage,^{12–14} cycloaddition, ring closure of the $-\text{C}=\text{C}-\text{C}=\text{O}$ moiety,^{15–18} and sigmatropic rearrangements.^{19,20} In comparison with the former three types of reactions, the sigmatropic rearrangement reactions of CH_2CHCOCl were subject to fewer

SCHEME 1: Photochemical 1,3-Cl Sigmatropic Rearrangement



studies. To the best of our knowledge, the photochemical reactions of its homologous compound, $\text{CH}_3\text{CHCHCOCl}$, have not been investigated before.

When irradiating CH_2CHCOCl in Ar matrix at 10 K with a high-pressure Hg lamp, Pietri et al.¹⁹ first observed the formation of the 1,3-Cl sigmatropic migration product, 3-chloro-1,2-propenone ($\text{ClCH}_2-\text{CH}=\text{C}=\text{O}$), with static FTIR spectroscopy. At longer wavelengths ($\lambda \geq 310$ nm), the 1,3-Cl sigmatropic migration was the only observed pathway. At shorter wavelengths ($\lambda \geq 230$ nm), smaller fragments (CO , HCl , CH_2CHCl , and C_2H_2) were observed as the final stable products in the FTIR spectrum since the rearrangement product $\text{ClCH}_2-\text{CH}=\text{C}=\text{O}$ was subject to secondary photodissociation under prolonged irradiation. Combined with MP2/6-31G* calculation, the photorearrangement was suggested to proceed in either the first excited S_1 state or the S_0 ground state following an internal conversion (IC).

More recently, the potential energy surfaces of isomerization and dissociation reactions for the CH_2CHCOCl in the S_0 , T_1 , T_2 , and S_1 states were mapped with DFT, CASSCF, MP2, and MR-CI calculations by Fang et al.²⁰ The T_1 , T_2 , and S_1 states were respectively characterized as ${}^3\pi\pi$, ${}^3n\pi$, and ${}^1n\pi$ in nature on the basis of the CASSCF wave functions and their electronic populations. It was found that there exists an $S_1/T_1/T_2$ three-surface intersection that should result in fast intersystem crossing. In addition, the 1,3-Cl sigmatropic migration barrier of $18.4 \text{ kcal mol}^{-1}$ in the T_1 state was shown to be significantly lower than that in the S_0 state, $41.8 \text{ kcal mol}^{-1}$. As a result, the calculation predicted that the photoinduced 1,3-Cl sigmatropic

* Corresponding author. E-mail: hongmei@iccas.ac.cn.

migration reaction probably follows a route in the T_1 state after an efficient intersystem crossing (ISC) of $S_1 \rightarrow T_1$.

As is known for the photochemistry of organic molecules, the reactive state is usually not the initially populated one. Ultrafast nonadiabatic transitions (IC or ISC) take place prior to the system's reaching the reactive state, through which favorable nonadiabatic reaction pathways are open.^{21,22} As far as the photoinduced 1,3-Cl sigmatropic migration reaction, several excited electronic states (S_1 , T_1 , and T_2) are all possibly involved. Which excited state does the reaction proceed through? Does the reaction proceed adiabatically in the S_1 state or nonadiabatically through crossing to the T_1 state? The answer appears controversial in the past experimental¹⁹ and theoretical²⁰ studies.

Another problem that has been ignored to some extent relates to the degree of concertedness of the reaction. Photochemical sigmatropic migration reactions have shown rigid stereochemistry and thus appear to proceed through a one-step concerted mechanism,²³ as assumed generally for pericyclic reactions. However, the possibility⁵ exists in any [1, n] migration that an alternate pathway through a stepwise mechanism involving radical dissociation-recombination (RDR) may compete to some extent with the concerted path.

In the present work, we have performed experimental and theoretical investigations into the photoinduced 1,3-Cl sigmatropic migration of CH_2CHCOCl and $\text{CH}_3\text{CHCHCOCl}$ in solution. Experimentally, the product formation is detected in real time, and the product yields are determined with time-resolved Fourier transform infrared (TR-FTIR) absorption spectroscopy. By monitoring the product yields varied with the laser excitation wavelength (193 and 266 nm) or the addition of triplet quencher, the photochemical rearrangement reaction is clarified to take place through the excited triplet state T_1 , but not the excited singlet state S_1 . Theoretically, the potential energy profiles of the rearrangement reaction in the T_1 and S_0 states are calculated at the B3LYP/cc-pVDZ level of theory, and the minimum energy crossing point on the T_1/S_0 intersection seam is located with the Newton-Lagrange method. Combined with the experimental determination, the reaction is elucidated to follow nonadiabatic pathways via two rapid ISC processes, $S_1 \rightarrow T_1$ and $T_1 \rightarrow S_0$, and the S_1/T_1 and T_1/S_0 surface intersections are found to play significant roles leading to the nonadiabatic pathways. Moreover, the theoretical calculations suggest that the photoinduced reaction of RCHCHCOCl ($R = \text{H}, \text{CH}_3$) proceeds through a stepwise mechanism involving radical dissociation-recombination, which is quite different from the generally assumed one-step concerted process for pericyclic reactions. The first step is the radical dissociation to form an intermolecular complex, INT, between Cl and RCHCHCO in the T_1 state. The second step is the recombination to form the final rearrangement product $\text{RCHClCH}=\text{C}=\text{O}$ in the ground S_0 state following the rapid $T_1 \rightarrow S_0$ ISC due to the T_1/S_0 surface intersection. Among all the possible reaction pathways, the nonadiabatic $S_1 \rightarrow T_1 \rightarrow S_0$ reaction pathway is the most favorable, corresponding to the lowest energy path.

2. Experimental and Computational Methods

2.1. Experiments. The photochemical reaction is monitored by step-scan TR-FTIR absorption spectroscopy.^{24,25} Step-scan FTIR spectrometers are commercially available but require significant modification for applications in a flash photolysis TRIR study. The TR-FTIR instrument (setup shown in Figure 1) comprises a Nicolet Nexus 870 step-scan FTIR spectrometer,

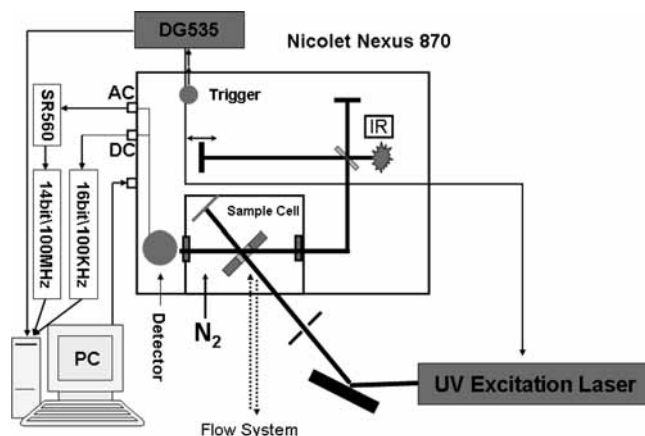


Figure 1. Schematic representation of the TR-FTIR experimental setup.

and a pulse generator (Stanford Research DG535) to initiate the laser pulse and achieve synchronization of the laser with data collection, two digitizers (internal 100 kHz, 16 bit digitizer and external 100 MHz, 14 bit GAGE CS14100 digitizer) that offer fast time resolution and a wide dynamic range as needed, and a personal computer to control the whole experiment. The detector used in this work is the photovoltaic MCT (0.5 mm) equipped with a fast internal preamplifier (50 MHz).

There are two outputs from the detector: output DC, corresponding to the value of the static interferogram; and output AC, corresponding to the time-resolved change of the interferogram. The AC signal was then amplified by an external preamplifier (Stanford Research, SR560). The differential absorbance spectra are calculated based on equation

$$\Delta A = A_{AC+DC} - A_{DC} = -\log_{10}(1 + \Delta I_{AC}/I_{DC}) \quad (1)$$

where I_{DC} and ΔI_{AC} are the single-beam intensity spectra corresponding to static (DC) and dynamic (AC) channels. ΔI_{AC} is calibrated before being used in an equation because a different gain is applied to the AC channel.^{24,25}

An ArF excimer laser (193 nm) or the fourth harmonic of a Nd:YAG laser (266 nm) operating at 10 Hz repetition rate was used in the experiments. The laser excitation beam was directed through an iris aperture (3 mm in diameter) and then overlapped with the infrared beam in the sample cell within the sample compartment of the FTIR spectrometer. The laser beam energy after the aperture was 5 mJ per pulse. A Harrick flowing solution cell with 2-mm-thick CaF_2 windows (path length: 100–500 μm) was used for the measurements.

CH_2CHCOCl (Alfa, >96%) and trans-1,3-pentadiene (TCI, >96%) were used without further purification. Chromatographic grade solvent (CH_3CN) was used, and a 1650–2200 cm^{-1} spectroscopic window was accessible for the TR-FTIR measurements.

The UV-visible absorption spectrum of the sample CH_2CHCOCl was recorded by a UV-vis spectrophotometer (model U-3010, Shimadzu).

2.2. Computational Methods. The geometries of the reactants, products, intermediates, and transition states along the reaction route in the T_1 or S_0 state were optimized using the hybrid density functional theory; that is, Becke's three-parameter nonlocal exchange functional with the nonlocal correlation functional of Lee, Yang, and Parr (B3LYP) with the cc-pVDZ basis sets.^{26,27} Harmonic vibrational frequencies, relative energies, and the zero-point energies were calculated at the same level with the optimized geometries. The intermediates were characterized by all the real frequencies. The transition states

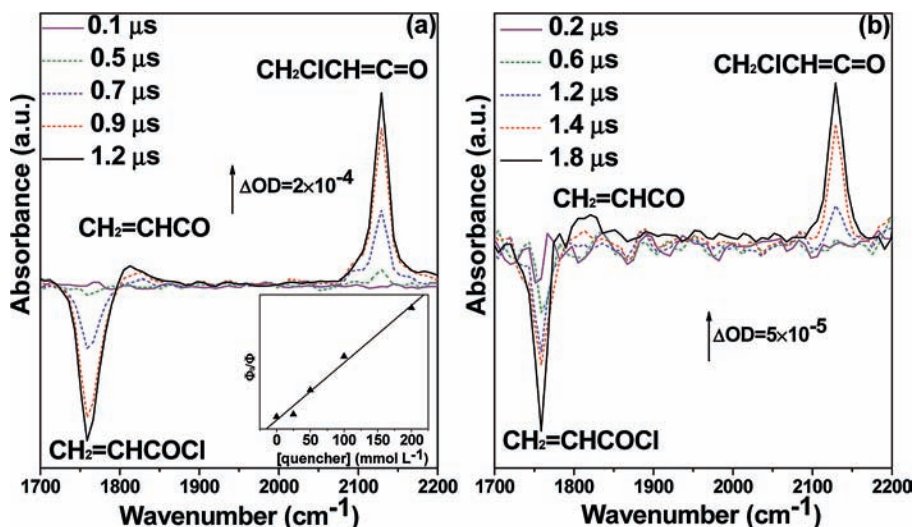


Figure 2. Infrared transient absorption spectra of 30 mM CH_2CHCOCl in CH_3CN solution following laser irradiation of (a) 193 nm and (b) 266 nm. Inset of panel a: Stern–Volmer plot when added with triplet quencher.

were confirmed by only one imaginary frequency. Connections of the transition states between two local minima have been confirmed by intrinsic reaction coordinate (IRC) calculations at the same level.²⁸

The minimum energy crossing point (MECP) on the intersection seam of the T_1 or S_0 states is located at the B3LYP/cc-pvdz level using the Newton–Lagrange method, which was introduced by Koga and Morokuma.²⁹ A homemade program was used for searching the MECP that has the lowest energy on the ($f-1$)-dimensional hypersurface of seam between two f -dimensional potential energy surfaces. This program has been used successfully to search the MECP of other reaction systems.^{30,31}

To aid spectral assignments, the IR frequencies and IR intensities for all the molecules of interest were calculated at the B3LYP/cc-pVDZ level. The polarized continuum model (PCM) was used to simulate the effect of the solvent (CH_3CN). The harmonic vibrational frequencies were scaled by a factor of 0.96. All of the theoretical calculations were performed with the Gaussian 03 program package.³²

3. Results and Discussion

3.1. Identification of the Photochemical Products. Figure 2 displays the TR-FTIR absorption spectra following 193 or 266 nm irradiation of the CH_2CHCOCl in CH_3CN solution. The negative band at 1760 cm^{-1} corresponds to the C=O stretch of the reactant CH_2CHCOCl , which undergoes photodepletion, whereas the two positive bands are due to the newly formed photoproducts. The strong band at 2128 cm^{-1} arises from the 1,3-Cl migration product, chloromethyl ketene ($\text{CH}_2\text{CICH}=\text{C}=\text{O}$). The weak band at 1813 cm^{-1} is attributed to the $\text{CH}_2=\text{CHCO}\cdot$ radical from the C–Cl bond fission reaction.

For the three transient infrared absorption bands observed in the TR-FTIR spectra in Figure 2, the spectral assignments are aided with the quantum chemical calculation at the B3LYP/cc-pVDZ level both in the gas phase and in the CH_3CN solution, and the calculated vibrational frequencies are shown in Table 1. The experimentally observed IR frequency for the stable parent molecule, CH_2CHCOCl , is measured to be 1760 cm^{-1} by static FTIR absorption spectra, which is very close to the calculated value, 1759 cm^{-1} , indicating the current level of calculation can provide accurate and reliable IR frequencies for

TABLE 1: IR Frequency and IR Intensity Calculated at the B3LYP/cc-pVDZ level^a

	gas phase		CH_3CN solution	
	ν (C=O) cm^{-1}	IR intensity km mol^{-1}	ν (C=O) cm^{-1}	IR intensity km mol^{-1}
CH_2CHCOCl	1788	322	1759	684
$\text{CH}_2\text{CHCO}\cdot$	1821	210	1792	418
CH_2CICHCO (T_1)	1722	128	1711	262
CH_2CICHCO (S_0)	2131	774	2094	1429

^a The harmonic vibrational frequencies are scaled by a factor of 0.96.

spectral assignment purposes. As shown in Table 1, the calculated IR frequencies for the two photoproducts, $\text{CH}_2=\text{CHCO}\cdot$ and $\text{CH}_2\text{CICH}=\text{C}=\text{O}$, agrees well with the experimentally observed spectral positions of 1813 and 2128 cm^{-1} , respectively. In addition, the typical absorption band of carbonyl radical³³ and ketene³⁴ are known to be around 1800 and 2100 cm^{-1} , further supporting these assignments. The 2128 cm^{-1} band observed in the transient infrared absorption spectra arises from the singlet product $\text{CH}_2\text{CICH}=\text{C}=\text{O}$, but not the triplet product $\text{CH}_2\text{CICH}=\text{C}=\text{O}$, because the latter corresponds to the IR absorption at much lower frequency, 1711 cm^{-1} .

3.2. Determination of the Product Yields. One advantage of the TR-FTIR absorption spectra is that it measures simultaneously the depletion of reactant molecules with the formation of photoproducts. Thus, both the amount of photoproduct formed and reactant consumed can be quantified by normalizing the peak area of the IR absorption band with the absorption coefficient. Although experimentally hard to determine, especially for transient species, the IR absorption coefficients can be acquired by ab initio calculations with the Gaussian program, which gives the IR intensity while computing the IR frequency of a specific vibrational mode, as shown in Table 1. The computed IR intensity in units of kilometers per mole actually denotes the integrated IR absorption coefficient.³⁵

The reaction occurs rapidly with both products and reactants simultaneously reaching their maximum spectral intensity at $1.2\text{ }\mu\text{s}$ (193 nm) or $1.8\text{ }\mu\text{s}$ (266 nm). The typical time evolution of the product and reactant band intensity is shown in Figure 3. As can be seen, the negative band corresponding to the reactant depletion recovers slightly at later time ($3.0\text{ }\mu\text{s}$) because some molecules populated to the T_1 state upon photoexcitation

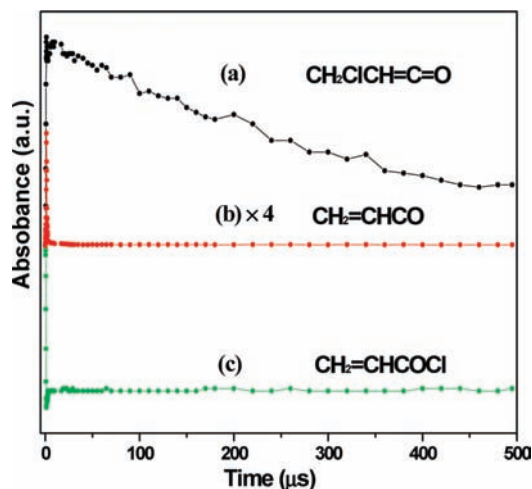


Figure 3. Kinetics curves for the transient infrared bands of (a) $\text{CH}_2\text{ClCH}=\text{C}=\text{O}$, (b) $\text{CH}_2=\text{CHCO}\cdot$, and (c) $\text{CH}_2=\text{CHCOCl}$ when irradiating 30 mM CH_2CHCOCl at 193 nm in CH_3CN solution.

undergo ISC to their ground state without chemical transformation. After 3.0 μs , the negative band sustains its intensity, reaching a plateau. The plateau intensity of the negative band should correspond to the actual consumption of the reactant due to photochemical reaction, although for the two photochemical products, the maximum intensities of the positive bands correspond to the product yields. At later time, the positive bands of photochemical products are decaying markedly due to some quenching process at a different rate. The $\text{CH}_2=\text{CHCO}\cdot$ radical decays within a few microseconds with predominantly second-order kinetics resulting from radical–radical recombination, whereas the stable product $\text{CH}_2\text{ClCH}=\text{C}=\text{O}$ decays within several hundreds of microseconds, with a lifetime of $283 \pm 24 \mu\text{s}$.

Adopting the positive bands of photoproducts with maximum intensity and the negative band of reactants with plateau intensity, both the amount of the photochemical product formation and the reactant consumption are quantified by normalizing the peak area of the IR absorption band with the absorption coefficient listed in Table 1. Furthermore, dividing the amount of photoproduct formation by reactant consumption gives the absolute yields for the two photochemical products of $\text{CH}_2=\text{CHCO}\cdot$ and $\text{CH}_2\text{ClCH}=\text{C}=\text{O}$, which is 0.32 and 0.66 respectively at 193 nm and 0.33 and 0.62 at 266 nm. Thus, the photochemical 1,3-Cl migration is shown to occur with equally good yields at both wavelengths, accounting for a much larger fraction yield than the α cleavage of the C–Cl bond in solution phase. Moreover, the sum of these two product yields is close to 1, indicating that the corresponding two reactions, the C–Cl fission and the 1,3-Cl migration, accounts for most of the photochemical reactions of CH_2CHCOCl in solution.

3.3. Identification of the Reactive Excited State. As an α , β unsaturated carbonyl compound containing the enone group $-\text{C}=\text{C}-\text{C}=\text{O}$, CH_2CHCOCl is a bichromophoric molecule that exhibits two absorption bands peaked at about 270 and 200 nm, as shown in Figure 4. The two excitation wavelengths used to initiate the photochemical reaction in this work, 266 and 193 nm, correspond to the dipole-forbidden transition to the $S_1(n\pi^*)$ state and the strongly dipole-allowed transition to the $S_2(\pi\pi^*)$ state, respectively. The S_2 state adiabatically correlates only with (energetically unavailable) highly excited photoproducts, and therefore, because no fluorescence is observed, it is assumed to rapidly internally convert to the lower lying S_1 state. As a result, CH_2CHCOCl molecules are shown to undergo identical pho-

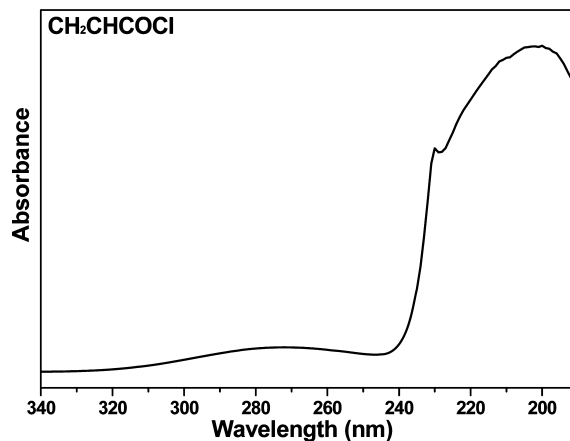


Figure 4. Gas phase UV–visible absorption spectrum of acryloyl chloride.

tochemical reactions upon S_2 state excitation by 193 nm and S_1 state excitation by 266 nm in our experiments. Several excited electronic states, the S_1 state and two lower triplet states, T_2 and T_1 , are possibly involved in the photoinduced 1,3-Cl migration reaction. Which excited state does the reaction proceed through?

Assuming the 1,3-Cl migration takes place through the S_1 or T_2 state, it requires surmounting a very high barrier. For example, relative to the S_0 zero level, the barrier in the S_1 state was estimated to be $121.8 \text{ kcal mol}^{-1}$ by the MP2/6-31G* calculation.²⁰ Such a high barrier can be overcome by 193 nm excitation ($145 \text{ kcal mol}^{-1}$) but not for 266 nm ($107 \text{ kcal mol}^{-1}$). However, our experiment shows that at 266 nm the 1,3-Cl migration occurs as efficiently as 193 nm with equal product yields as described in Section 3.2. This indicates that the reaction does not proceed in either the S_1 or T_2 state because otherwise, the reaction will be prohibited at 266 nm due to the inaccessible barrier height. Instead, the reaction should occur through the lower T_1 state.

To ascertain whether the 1,3-Cl migration proceeds through the T_1 state, the photochemical reaction was performed in the presence of the triplet quencher, trans-1,3-pentadiene. Assuming the reaction occurs through the T_1 state, the quencher addition is expected to lower the yield of CH_2ClCHCO . Indeed, the product yield decreased as the concentration of quencher increased. It is generally assumed that if only one excited state is involved in a photochemical reaction, a Stern–Volmer plot of ϕ_0/ϕ (where ϕ_0 is the quantum yield of the reaction and ϕ is the quantum yield in the presence of quencher; both can be determined from TR-FTIR spectra) vs the quencher concentration shows a straight line.²³ Actually, an excellent linear correlation ($R^2 = 0.9842$) is obtained with the Stern–Volmer plot, as shown in the Figure 2a inset. This result clearly suggests that, although several excited electronic states may be possibly involved, most (if not all) of the photoinduced 1,3-Cl migration reaction occurs through the T_1 state. On the other hand, for the competing C–Cl bond fission reaction which has been known to occur in the excited singlet state S_1 ,^{12,20} the yield of its product $\text{CH}_2=\text{CHCO}\cdot$ is observed not to vary with the addition of the triplet quencher.

3.4. An Additional Study: the Photochemical Reaction of $\text{CH}_3\text{CHCHCOCl}$. For another α , β unsaturated carbonyl compound, $\text{CH}_3\text{CHCHCOCl}$, we have also performed transient infrared absorption measurements to reveal its photochemical products and reactive excited state. As shown in Figure 5, two photochemical products can be identified. One is the

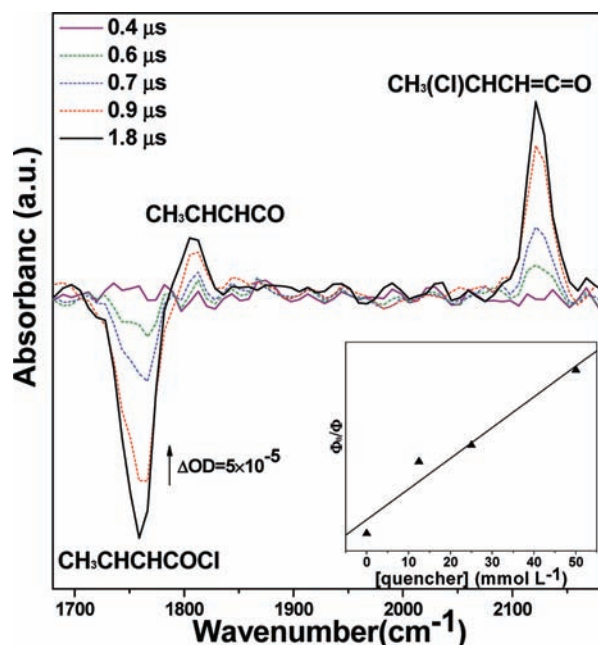


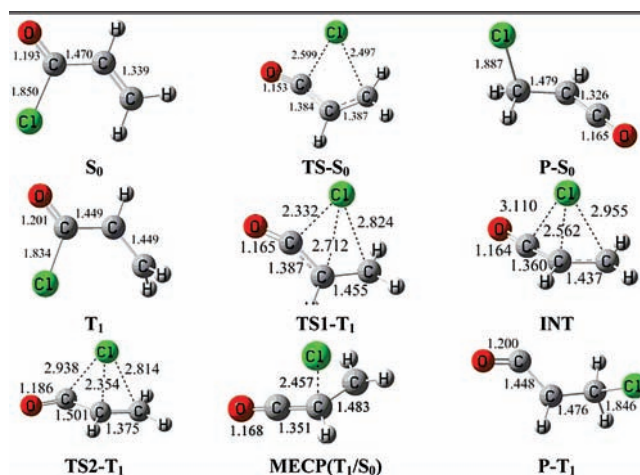
Figure 5. Infrared transient absorption spectra of 30 mM $\text{CH}_3\text{CHCHCOCl}$ solution in CH_3CN following laser irradiation of 193 nm. Inset: Stern–Volmer plot when added with triplet quencher.

$\text{CH}_3\text{CH}=\text{CHCO}\cdot$ radical arising from the C–Cl bond fission reaction, and the other is the rearrangement product $\text{CH}_3(\text{Cl})\text{CHCH}=\text{C}=\text{O}$ due to the 1,3-Cl migration. With the addition of the triplet quencher, trans-1,3-pentadiene, the product yield of $\text{CH}_3(\text{Cl})\text{CHCH}=\text{C}=\text{O}$ decreased, and the Stern–Volmer plot of ϕ_0/ϕ vs the quencher concentration showed an excellent linear correlation, as displayed in the inset of Figure 5. This indicates that the photoinduced 1,3-Cl migration reaction of $\text{CH}_3\text{CHCHCOCl}$ also occurs through the T_1 state. In contrast, the yield of the other product, $\text{CH}_3\text{CH}=\text{CHCO}\cdot$, is shown not to be dependent on the addition of the triplet quencher because the C–Cl bond fission reaction correlates to a singlet state. Overall, the compound $\text{CH}_3\text{CHCHCOCl}$ undergoes photochemical reactions similar to its homologous counterpart, CH_2CHCOCl , consisting of the C–Cl bond fission channel and the 1,3-Cl migration channel. The only difference is that $\text{CH}_3\text{CHCHCOCl}$ shows a slightly decreased product yield of the 1,3-Cl migration channel, which is determined to be 0.43, as compared to that of 0.66 in the case of CH_2CHCOCl .

With one methyl group substituted to the ethylenic C=C bond, the internal conversion $S_1 \rightarrow S_0$ of $\text{CH}_3\text{CHCHCOCl}$ is expected to increase its rate as compared to that of CH_2CHCOCl due to the increased density of states. As a result, the internal conversion $S_1 \rightarrow S_0$ should compete more strongly with the intersystem crossing $S_1 \rightarrow T_1$ for the excited $\text{CH}_3\text{CHCHCOCl}$ molecules. Thus, the branching ratio of the 1,3-Cl migration reaction proceeding through the T_1 state is reduced for the $\text{CH}_3\text{CHCHCOCl}$ molecules as compared to that for CH_2CHCOCl molecules, as observed in our experiment. This demonstrates from another aspect that the 1,3-Cl migration reaction takes place through the T_1 state following the ISC of $S_1 \rightarrow T_1$, in which case its product yield can be lowered when the competing internal conversion $S_1 \rightarrow S_0$ increases its rate as for a larger system, $\text{CH}_3\text{CHCHCOCl}$.

3.5. Stepwise Reaction Mechanisms in T_1 State. Since our experiments suggest strongly that the 1,3-Cl migration reaction proceeds through T_1 state, we performed quantum chemical calculations to reveal the detailed reaction paths in the T_1 state.

TABLE 2: Optimized Geometries of Reactants, Intermediates, Transition States, and Products for the 1,3-Cl Sigmatropic Migration of $\text{CH}_2=\text{CHCOCl}$ in the T_1 and S_0 States at the Level of B3LYP/cc-pVDZ^a



^a The optimized geometry of the minimal energy crossing point of the T_1/S_0 surface intersection MECP (T_1/S_0) at the B3LYP/cc-pVDZ level. Bond lengths are in angstroms.

We also calculated the reaction occurring in the ground S_0 state to compare if there are any different reaction mechanisms for these two states. Both reaction paths are calculated at the B3LYP/cc-pVDZ level of theory, which is a reliable method to locate the stationary points and their relative energies in the ground singlet S_0 and triplet T_1 states.

Table 2 lists all the optimized stationary structures along the S_0 and T_1 reaction pathways, and the corresponding energies obtained are displayed in Figure 6. In the ground S_0 state, the reaction follows a one-step concerted mechanism as generally assumed for pericyclic reactions, through one four-membered cyclic transition state and surmounting a reaction barrier of 38.6 kcal mol⁻¹. However, the reaction proceeds through a distinctively different mechanism in the triplet T_1 state. As shown in Figure 6 and Table 2, our calculation locates explicitly a 6.8 kcal mol⁻¹ local potential-energy minimum INT along the T_1 state pathway. This reveals that the photochemical 1,3-Cl migration proceeds through a stepwise mechanism in the T_1 state, which behaves like a radical dissociation-recombination process; that is, while first detached from C_1 atom, the Cl atom approaches the C_2 atom, forming the weakly interacted radical pair complex INT and then migrating to the C_3 atom to form the final product, chloromethyl ketene. The 6.8 kcal mol⁻¹ local potential-energy minimum corresponds to a short-lived transient intermediate INT that can be described as a weakly π -interacted radical pair between Cl and CH_2CHCO . The detached Cl atom is not completely free, but still attracted to the C_2 atom in the radical pair complex INT. After a short stagnation in this 6.8 kcal mol⁻¹ local potential-energy minimum, the Cl atom continues to migrate onto the C_3 atom, forming the final product chloromethyl ketene. Thus, the reaction route in the T_1 state can be regarded as a stepwise radical dissociation–recombination process. We performed MP2/cc-pVDZ calculations in which the T_1 intermediate INT can also be located, corresponding to a 5.0 kcal mol⁻¹ local minimum and a structure very close to that obtained from B3LYP/cc-pVDZ. This gives further evidence for the existence of the T_1 intermediate INT and the stepwise mechanism.

For the 1,3-Cl migration reaction of CH_2CHCOCl in the T_1 state, only one transition state was revealed in the calculation

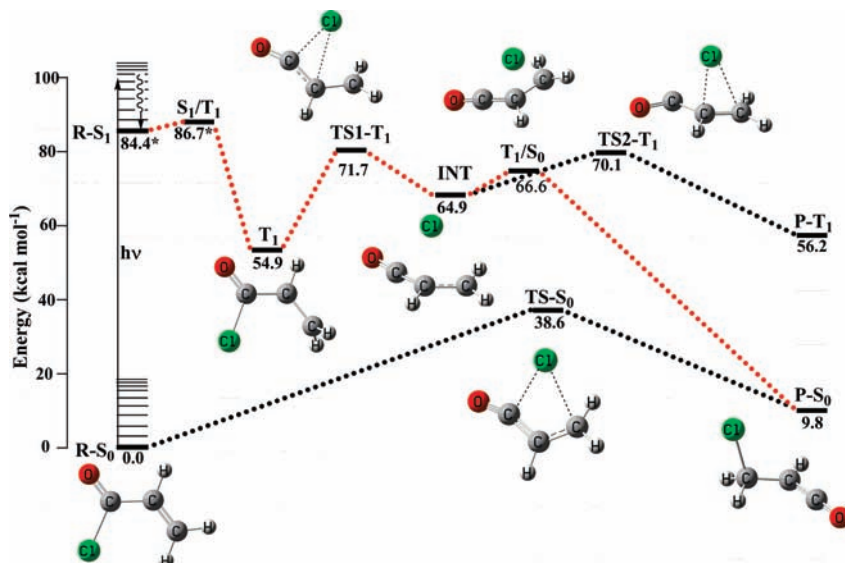


Figure 6. Energy profiles along an arbitrary reaction coordinate showing the 1,3-Cl migration reaction pathway of $\text{CH}_2=\text{CHCOCl}$. Relative energy values are obtained from the B3LYP/cc-pVDZ calculations with the total energies corrected by ZPVE. The T_1/S_0 surface intersection is located with the Newton–Lagrange method at the B3LYP/cc-pVDZ level. The red dotted lines denote the lowest energy reaction pathway. The asterisk (*) denotes that adiabatic excitation energy of the S_1 state and the S_1/T_1 surface intersection energy values are taken from ref 20.

by Fang et al.²⁰ The single point energy was calculated with the method of MR-CI using the B3LYP/cc-pVDZ optimized geometries. Although the absolute single point energies were probably more accurately obtained, their calculation did not locate all the stationary points, including the local potential-energy minimum INT along the reaction path in the T_1 state, and thus did not reveal the stepwise radical dissociation–recombination mechanism, probably because the IRC calculations to confirm the transition states linking two local minima were not carefully performed.

In addition to the mechanistic information, the current B3LYP/cc-pVDZ level of calculation can also provide reliable energetic information for the 1,3-Cl migration reaction in the T_1 and S_0 states. The reaction barrier in the T_1 and S_0 states obtained by the current B3LYP calculation (16.8 kcal mol⁻¹ and 38.6 kcal mol⁻¹, respectively) actually agrees with Fang's²⁰ results of 18.4 kcal mol⁻¹ and 41.8 kcal mol⁻¹ by MR-CI single point energy calculations.

Why does the photochemical 1,3-Cl migration reaction in the T_1 state take a stepwise mechanism that is totally different from the one-step concerted pericyclic process of the thermal migration in the S_0 state? We speculate that the origin of this difference may be ascribed to the biradicaloid nature of the T_1 state. Since the T_1 state of $\text{CH}_2=\text{CHCOCl}$ originates from the $\text{C}=\text{C} \pi \rightarrow \pi^*$ excitation, the ethylenic bond becomes a single bond, and the two carbon atoms are partitioned with unpaired electrons, which could attract the migrating Cl atom to combine with each of them step-by-step. This results in a stepwise process for the 1,3-Cl migration reaction: that is, after detached from the C_1 atom, the Cl atom first approaches the ethylenic C_2 atom, forming the weakly interacted complex INT, and then migrates to bond with the ethylenic C_3 atom forming the final rearrangement product.

This effect caused by the biradicaloid T_1 state becomes more pronounced for another α, β unsaturated carbonyl compound, $\text{CH}_3\text{CH}=\text{CHCOCl}$, when the C_2 atom is partitioned with more electron density because of the CH_3 conjugation. As shown in Figure 7 and Table 3, the transient intermediate INT along the stepwise T_1 reaction pathway of $\text{CH}_3\text{CH}=\text{CHCOCl}$ actually corresponds to a radical pair complex with an increased binding

energy of 7.4 kcal mol⁻¹. Here, the detached Cl atom approaches the C_2 atom more closely, nearly forming a $\text{C}_2\text{--Cl}$ bond, with the bond length to be 1.96 Å.

Except for the stepwise reaction mechanism, another noticeable fact shown here is that the reaction barrier in the T_1 state of these α, β unsaturated carbonyl compounds ($\text{CH}_2=\text{CHCOCl}$ and $\text{CH}_3\text{CH}=\text{CHCOCl}$) is greatly lowered as compared to that in the S_0 state. One reason is that the reaction in the T_1 state proceeds stepwisely, which is generally much easier than the concerted reaction process that the S_0 state follows. Another reason should be due to the extra driving force provided by the ethylenic unpaired electrons of the $\text{C}=\text{C} \pi \rightarrow \pi^*$ excited T_1 state, which facilitates the 1,3-Cl migration remarkably, whereas for the two upper S_1 and T_2 states originating from the $\text{C}=\text{O} n \rightarrow \pi^*$ excitation, there is no such extra driving force to facilitate the 1,3-Cl migration. Thus, it is expected that the reactions in the S_1 and T_2 states require surmounting high barriers. Assuming the barriers in the S_1 and T_2 states are identical to that in the S_0 state (calculated to be 41.8 kcal mol⁻¹ by Fang²⁰) and adding this barrier to the adiabatic excitation energy of these two states (calculated to be 84.4 kcal mol⁻¹ for S_1 and 80.8 kcal mol⁻¹ for T_2 by Fang²⁰), the transition states can be estimated to locate 126.2 and 122.6 kcal mol⁻¹ above the S_0 zero level for the S_1 and T_2 states, respectively. Actually, this estimation should be quite reasonable, since previous MP2/6-31G* calculation¹⁹ also estimated a 121.8 kcal mol⁻¹ transition state in the S_1 state relative to the S_0 zero level. Overall, among the four possibly involved electronic states (the S_1 , T_2 , T_1 , and S_0 states), the stepwise reaction in the T_1 state requires surmounting the lowest reaction barrier. This is probably one of the reasons why the photochemical rearrangement reaction occurs through the T_1 state, as has been demonstrated in our experiments.

As observed in the experiment (Figure 2), there is a C--Cl bond fission reaction known to proceed in the S_1 state^{12,20} competing with the 1,3-Cl migration reaction through the T_1 state. One might think that the 1,3-Cl migration product CH_2ClCHCO could also be produced if the completely dissociated Cl atom through the C--Cl bond fission reaction recombines with its cofragment $\text{CH}_2\text{CHCO}\cdot$ radical in the solvent cage. If this is the case, the product yield of CH_2ClCHCO should not

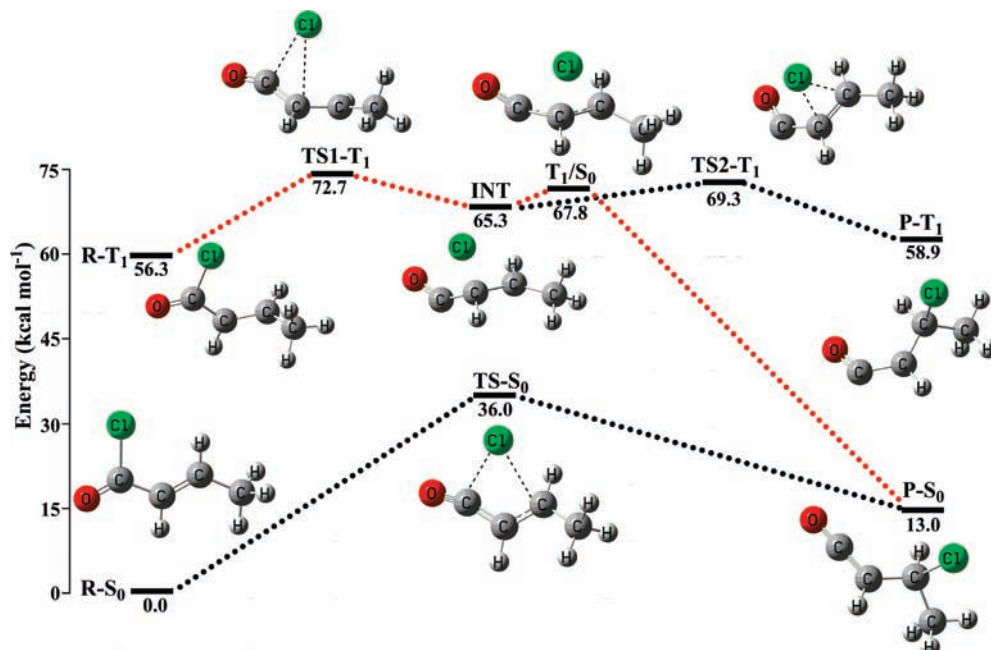
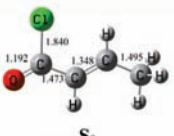
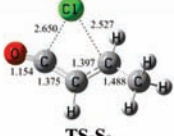
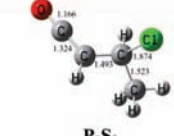
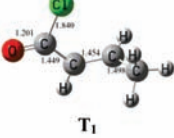
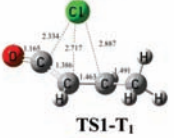
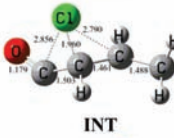
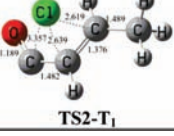
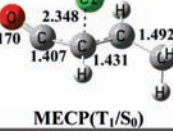
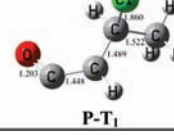


Figure 7. Energy profiles along an arbitrary reaction coordinate showing the 1,3-Cl migration reaction pathway of $\text{CH}_3\text{CH}=\text{CHCOCl}$. Relative energy values are obtained from the ZPVE-corrected B3LYP/cc-pVDZ total energies. The T_1/S_0 surface intersection is located with the Newton–Lagrange method at the B3LYP/cc-pVDZ level. The red dotted lines denote the lowest-energy reaction pathway.

TABLE 3: Optimized Geometries of Reactants, Intermediates, Transition States, and Products for the 1,3-Cl Sigmatropic Migration of $\text{CH}_3\text{CH}=\text{CHCOCl}$ in the T_1 and S_0 States at the Level of B3LYP/cc-pVDZ^a

 S ₀	 TS-S ₀	 P-S ₀
 T ₁	 TS1-T ₁	 INT
 TS2-T ₁	 MECP(T ₁ /S ₀)	 P-T ₁

^a The optimized geometry of the minimal energy crossing point of the T_1/S_0 surface intersection MECP (T_1/S_0) at the B3LYP/cc-pVDZ level. Bond lengths are in angstroms.

correlate with the addition of a triplet quencher because the C–Cl bond fission reaction occurs in the S_1 state.^{12,20} In contrast, our experiment (Figure 2 inset) has shown that the product yield of CH_2ClCHCO decreased markedly with the addition of the triplet quencher, strongly suggesting that the reaction correlates to the T_1 state, and the rearrangement product CH_2ClCHCO is not formed through the completely dissociated Cl atom's recombining with its cofragment $\text{CH}_2\text{CHCO}\cdot$ radical in the solvent cage. Such a radical recombination following the C–Cl bond fission most likely leads back to their precursor CH_2CHCOCl , but not the rearranged product CH_2ClCHCO .

3.6. Nonadiabatic Reaction Pathway. As suggested by our experiments and theoretical calculations, the photoinduced 1,3-Cl migration reaction proceeds through the T_1 state. On the other hand, considering the fact that the final products probed in the

transient infrared absorption spectra are in their ground S_0 states, there may exist T_1/S_0 surface intersections that lead to inter-system crossing from T_1 to S_0 along the reaction path. We performed further calculations to explore the possible T_1/S_0 surface intersection using the Newton–Lagrange method introduced by Koga and Morokuma²⁹ at the B3LYP/cc-pVDZ level. Our calculation shows that there is, indeed, surface intersection between the T_1 and S_0 states for both reaction systems of $\text{CH}_2=\text{CHCOCl}$ and $\text{CH}_3\text{CH}=\text{CHCOCl}$. The minimum energy crossing point (MECP), which has the same geometry and energy for the singlet and triplet states, is located on the intersection seam. The optimized geometries of MECP for the reaction systems of $\text{CH}_2=\text{CHCOCl}$ and $\text{CH}_3\text{CH}=\text{CHCOCl}$ are shown separately in Tables 2 and 3, and their energy values are given separately in Figures 6 and 7. For $\text{CH}_2=\text{CHCOCl}$, the energy of MECP is only 1.7 kcal mol⁻¹ above the T_1 intermediate INT. For $\text{CH}_3\text{CH}=\text{CHCOCl}$, the MECP lies 2.5 kcal mol⁻¹ above the T_1 intermediate INT in energy. For the two reaction systems, the energies and geometries of the MECP (T_1/S_0) are both very close to the T_1 intermediate INT. Consequently, it is expected that the $T_1 \rightarrow S_0$ ISC can occur efficiently in the INT region, and the subsequent reaction processes can proceed along the ground-state pathway.

Overall, it can be established from the above experiments and calculations that the photoinduced 1,3-Cl migration of $\text{CH}_2=\text{CHCOCl}$ proceeds through a nonadiabatic reaction pathway comprising two efficient ISC processes, $S_1 \rightarrow T_1$ and $T_1 \rightarrow S_0$, as highlighted with the red dotted lines in Figure 6. In solution, the excited hot $S_1(\nu)$ molecules are deactivated efficiently to the S_1 zero level through vibrational relaxation, which occurs within picoseconds or faster. Once in the S_1 zero level, the molecules just fall into the proximity of the S_1/T_1 surface intersection calculated to be only 2.3 kcal mol⁻¹ above the S_1 minimum,²⁰ where ISC becomes dominant over IC,²⁰ resulting in efficient depopulation of molecules to the T_1 state. Subsequently, the 1,3-Cl migration proceeds through a stepwise radical dissociation–recombination process. The first step is the

radical dissociation, forming an intermolecular complex INT between Cl and CH₂CHCO in the T₁ state. The second step is the recombination forming the final rearrangement product CH₂ClCH=C=O in the ground S₀ state following the rapid T₁ → S₀ ISC in the INT region, which is very close to the T₁/S₀ surface intersection (calculated to be only 1.7 kcal mol⁻¹ above the T₁ INT). The recombination process requires surmounting a very low barrier of only 1.7 kcal mol⁻¹ if considering the MECP (T₁/S₀) as a transition state and thus proceeds more favorably in the ground S₀ state than in the T₁ state. Basically, it is shown here that the S₁/T₁ and T₁/S₀ surface intersections facilitate greatly the corresponding ISC processes of S₁ → T₁ and T₁ → S₀ and, thus, play significant roles resulting in nonadiabatic pathways for the photoinduced 1,3-Cl migration of CH₂=CHCOCl. For the CH₃CHCHCOCl system, the photoinduced 1,3-Cl migration also undergoes nonadiabatic reaction pathways via intersystem crossing similar to its homologous counterpart, CH₂CHCOCl, as shown with the red dotted lines in Figure 7.

The nonadiabatic reaction pathway of S₁ → T₁ → S₀ is only rate-limited by the barrier of 16.8 kcal mol⁻¹ when forming the intermolecular complex INT. It is likely that the reaction can also occur directly through the internal conversion of S₁ → S₀, as postulated by Pietri et al.¹⁹ But in that case, the reaction requires surmounting a much higher barrier of 38.6 kcal mol⁻¹ after passing to the ground S₀ state. Among all the possible reaction pathways, the nonadiabatic reaction pathway of S₁ → T₁ → S₀ corresponds to the lowest energy path and therefore should be the most favorable energetically. In addition, the excited S₁(*v*) molecules are deactivated efficiently into the S₁/T₁ intersection proximity through solvent vibrational relaxation, where the ISC of S₁ → T₁ is greatly facilitated and becomes dominant over the IC of S₁ → S₀. As a matter of fact, the key participation of T₁ state in the nonadiabatic reaction pathway is clearly evidenced by our experiment, which shows that the product yield decreases with the addition of triplet quencher, and the Stern–Volmer plot of ϕ_0/ϕ vs the quencher concentration exhibits an excellent linear correlation.

Our experimental identification of the T₁ state as the reactive excited state agrees with Fang's theoretical calculations,²⁰ which also suggested that the rearrangement reaction proceeds more easily along the T₁ pathway than in the S₀ state because of the significantly lowered reaction barrier in the T₁ state. Furthermore, we performed more comprehensive calculations, which suggest that the reaction actually follows a nonadiabatic S₁ → T₁ → S₀ reaction pathway and proceeds through a stepwise T₁ radical dissociation–S₀ recombination mechanism. Our calculations have located the intermolecular reaction complex INT in the T₁ state as well as the T₁/S₀ surface intersection close to the INT region.

4. Conclusion

Taking the two α , β unsaturated carbonyl compounds (CH₂CHCOCl and CH₃CHCHCOCl) as model systems, we have examined the reaction dynamics of the photochemical 1,3-Cl sigmatropic rearrangements in solution and provided mechanistic insights into this important pericyclic reaction. Experimentally, the rearrangement product formation is detected in real time, and the product yields are determined with the time-resolved Fourier transform infrared absorption spectroscopy. The control experiments monitoring the product yields varied with the laser excitation wavelength (193 and 266 nm) or the addition of triplet quencher suggest strongly that the photoinduced 1,3-Cl migration proceeds through the excited triplet state T₁, but not the excited

S₁ or T₂ state. Theoretically, the potential energy profiles of the rearrangement reaction in the T₁ and S₀ states are calculated at the B3LYP/cc-pVDZ level of theory, and the minimum energy crossing point on the T₁/S₀ intersection seam is located with the Newton–Lagrange method. Combined with the experimental observation, the reaction is elucidated to follow nonadiabatic pathways via two rapid ISC processes, S₁ → T₁ and T₁ → S₀. The S₁/T₁ and T₁/S₀ surface intersections greatly facilitate the corresponding ISC processes and, thus, play significant roles, resulting in nonadiabatic pathways.

Among all the possible reaction pathways, the nonadiabatic S₁ → T₁ → S₀ reaction pathway is the most favorable, corresponding to the lowest energy path. The possible pathway through the IC of S₁ → S₀ is less favorable due to the much higher barrier after passing to the ground S₀ state. The key participation of the T₁ state in the nonadiabatic S₁ → T₁ → S₀ reaction pathway is strongly evidenced by the experiment that shows that the product yield decreases with the addition of triplet quencher, and the Stern–Volmer plot of ϕ_0/ϕ vs the quencher concentration exhibits an excellent linear correlation.

Moreover, the theoretical calculations have located the intermolecular reaction complex INT in the T₁ state and the T₁/S₀ surface intersection close to the INT region, suggesting that the photoinduced reaction of RCHCHCOCl (R = H, CH₃) occurs through a stepwise mechanism involving radical dissociation–recombination that is quite different from the generally assumed one-step concerted process for pericyclic reactions. The first step is the radical dissociation, forming an intermolecular complex INT between Cl and RCHCHCO in the T₁ state. The second step is the recombination forming the final rearrangement product RCHClCH=C=O in the ground S₀ state following the rapid T₁ → S₀ ISC due to the T₁/S₀ surface intersection.

Acknowledgment. This work is financially supported by the National Natural Science Foundation of China (Grants nos. 20733005 and 20673126), the National Basic Research Program of China (2007CB815200, 2007AA02Z116), and the Chinese Academy of Sciences. The authors are thankful to Prof. W. H. Fang for the valuable discussion with the theoretical calculation results.

References and Notes

- (1) Woodward, R. B.; Hoffmann, R. *The Conservation of Orbital Symmetry*; Verlag Chemie GmbH/Academic Press: Weinheim/Bergstr., 1970.
- (2) Hoffmann, R.; Woodward, R. B. *Acc. Chem. Res.* **1968**, *1*, 17.
- (3) Frey, H. M.; Walsh, R. *Chem. Rev.* **1969**, *69*, 103.
- (4) Singh, J. *Photochemistry and Pericyclic Reactions*; New Age International: New Delhi, India, 2005.
- (5) Spangler, C. W. *Chem. Rev.* **1976**, *76*, 187.
- (6) Breslow, R.; Canary, J. W. *J. Am. Chem. Soc.* **1991**, *113*, 3950.
- (7) Bibas, H.; Wong, M. W.; Wentrup, C. *J. Am. Chem. Soc.* **1995**, *117*, 9582.
- (8) Koch, R.; Wong, M. W.; Wentrup, C. *J. Org. Chem.* **1996**, *61*, 6809.
- (9) Zhdankin, V. V.; Stang, P. J. *Chem. Rev.* **2008**, *108*, 5299.
- (10) Wortelboer, H. M.; Usta, M.; Zanden, J. J.; Bladeren, P. J.; Rietjens, I. M. C. M.; Cnubben, N. H. P. *Biochem. Pharmacol.* **2005**, *69*, 1879.
- (11) Billard, T. *Chem.—Eur. J.* **2006**, *12*, 975.
- (12) Arendt, M. F.; Browning, P. W.; Butler, L. J. *J. Chem. Phys.* **1995**, *103*, 5877.
- (13) Szpunar, D. E.; Miller, J. L.; Butler, L. J.; Qi, F. *J. Chem. Phys.* **2004**, *120*, 4223.
- (14) Lau, K. C.; Liu, Y.; Butler, L. J. *J. Chem. Phys.* **2005**, *123*, 054322.
- (15) Bonneau, R. *J. Am. Chem. Soc.* **1980**, *102*, 3816.
- (16) Schuster, D. I. In *The chemistry of enones*; Patai, S., Rappoport, Z., Eds.; John Wiley and Sons: Chichester, U.K., 1989; Vol. 2, pp 693–756.
- (17) Guerin, D. J.; Miller, S. J. *J. Am. Chem. Soc.* **2002**, *124*, 2134.

- (18) Wilsey, S.; González, L.; Robb, M. A.; Houk, K. N. *J. Am. Chem. Soc.* **2000**, *122*, 5866.
- (19) Pietri, N.; Monnier, M.; Aycard, J. P. *J. Org. Chem.* **1998**, *63*, 2462.
- (20) Cui, G.; Li, Q.; Zhang, F.; Fang, W.; Yu, J. *J. Phys. Chem. A* **2006**, *110*, 11839.
- (21) Gloaguen, E.; Mestdagh, J. M.; Poisson, L.; Lepetit, F.; Visticot, J. P.; Soep, B.; Coroiu, M.; Eppink, A.; Parker, D. H. *J. Am. Chem. Soc.* **2005**, *127*, 16529.
- (22) Poisson, L.; Raffael, K. D.; Soep, B.; Mestdagh, J. M.; Buntinx, G. *J. Am. Chem. Soc.* **2006**, *128*, 3169.
- (23) Turro, N. J. *Modern Molecular Photochemistry*; University Science Books: Sausalito, CA, 1991.
- (24) Uhmann, W.; Becker, A.; Taran, C.; Siebert, F. *Appl. Spectrosc.* **1991**, *45*, 390.
- (25) Special section on time-resolved, step-scan FT-IR spectroscopy. *Appl. Spectrosc.* **1997**, *54*, April issue.
- (26) Becke, A. D. *J. Chem. Phys.* **1993**, *98*, 5648.
- (27) Lee, C.; Yang, W.; Parr, R. G. *Phys. Rev. B: Condens. Matter Mater. Phys.* **1988**, *37*, 785.
- (28) Gonzalez, C.; Schlegel, H. B. *J. Phys. Chem.* **1990**, *94*, 5523.
- (29) Koga, N.; Morokuma, K. *Chem. Phys. Lett.* **1985**, *119*, 371.
- (30) Zhao, H. M.; Bian, W. S.; Liu, K. *J. Phys. Chem. A* **2006**, *110*, 7858.
- (31) Zhao, S. L.; Wu, W. Q.; Zhao, H. M.; Wang, H.; Yang, C. F.; Liu, K. H.; Su, H. M. *J. Phys. Chem. A* **2009**, *113*, 23.
- (32) Frisch, M. J.; Trucks, G. W.; Schlegel, H. B.; Scuseria, G. E.; Robb, M. A.; Cheeseman, J. R.; Montgomery, J. A., Jr.; Vreven, T.; Kudin, K. N.; Burant, J. C.; Millam, J. M.; Iyengar, S. S.; Tomasi, J.; Barone, V.; Mennucci, B.; Cossi, M.; Scalmani, G.; Rega, N.; Petersson, G. A.; Nakatsuji, H.; Hada, M.; Ehara, M.; Toyota, K.; Fukuda, R.; Hasegawa, J.; Ishida, M.; Nakajima, T.; Honda, Y.; Kitao, O.; Nakai, H.; Klene, M.; Li, X.; Knox, J. E.; Hratchian, H. P.; Cross, J. B.; Bakken, V.; Adamo, C.; Jaramillo, J.; Gomperts, R.; Stratmann, R. E.; Yazyev, O.; Austin, A. J.; Cammi, R.; Pomelli, C.; Ochterski, J. W.; Ayala, P. Y.; Morokuma, K.; Voth, G. A.; Salvador, P.; Dannenberg, J. J.; Zakrzewski, V. G.; Dapprich, S.; Daniels, A. D.; Strain, M. C.; Farkas, O.; Malick, D. K.; Rabuck, A. D.; Raghavachari, K.; Foresman, J. B.; Ortiz, J. V.; Cui, Q.; Baboul, A. G.; Clifford, S.; Cioslowski, J.; Stefanov, B. B.; Liu, G.; Liashenko, A.; Piskorz, P.; Komaromi, I.; Martin, R. L.; Fox, D. J.; Keith, T.; Al-Laham, M. A.; Peng, C. Y.; Nanayakkara, A.; Challacombe, M.; Gill, P. M. W.; Johnson, B.; Chen, W.; Wong, M. W.; Gonzalez, C.; Pople, J. A. *Gaussian 03, revision B.03*; Gaussian, Inc.: Wallingford, CT, 2004.
- (33) Neville, A. G.; Brown, C. E.; Rayner, D. M.; Luszyk, J.; Ingold, K. U. *J. Am. Chem. Soc.* **1991**, *113*, 1869.
- (34) Lin-Vien, D.; Cothup, N. B.; Fateley, W. G.; Graselli, J. G. *The Handbook of Infrared and Raman Characteristic Frequencies of Organic Molecules*; Academic: San Diego, CA, 1991.
- (35) Hess, B. A.; Schaad, L. J. *Chem. Rev.* **1986**, *86*, 709.

JP906583U